

Cite this: *Mater. Adv.*, 2025,  
6, 9209

# Mapping the energy landscape of a supramolecular system *via* time-resolved asymmetric-flow field flow fractionation

Maria Kariuki,<sup>a</sup> Julia Y. Rho <sup>b</sup> and Sébastien Perrier <sup>\*abc</sup>

The optimisation of the design and preparation of supramolecular systems for targeted functions requires a comprehensive understanding of the self-assembly energy landscape, including the full spectrum of its pathway complexity. We propose here a general strategy to map this energy landscape, involving the monitoring of the formation and evolution of structures generated during self-assembly. As a demonstration of its utility, we applied this approach to a self-assembling cyclic peptide–polymer conjugate system, where assembly is governed by the interplay between  $\beta$ -sheet hydrogen bonding and secondary hydrophobic interactions. Using asymmetric flow field-flow fractionation (AF4), we gained key thermodynamic insights into this system, showing that equilibrium is reached through the formation of nanotubular assemblies stabilized by hydrogen bonding. Moreover, the complexity of the assembly pathways was found to be directly influenced by both the molecular design and the preparation protocol. These factors critically determine whether the system follows the thermodynamically favoured H-bonding route or is diverted into a competing kinetic pathway dominated by the hydrophobic effect. The latter leads to the formation of metastable disordered aggregates, which delay or obstruct the emergence of well-defined nanotube structures due to the inherently slow disassembly dynamics of the system. We show that clarifying this three-way relationship between pathway, molecular design, and preparation method is a pivotal step towards regulating pathway selection and achieving precise control over the final outcome of supramolecular self-assembly.

Received 11th August 2025,  
Accepted 19th October 2025

DOI: 10.1039/d5ma00887e

rsc.li/materials-advances

## 1. Introduction

The effective design of supramolecular materials is driven by insights into the energy landscapes that govern self-assembly processes under various conditions.<sup>1–8</sup> This approach relies on identifying both the thermodynamic and kinetic states that supramolecular structures can adopt during polymerisation. Thermodynamically controlled assemblies correspond to the global minimum on the free energy landscape and remain stable over time without undergoing further reorganisation, hence they are considered to be at equilibrium.<sup>9–12</sup> In contrast, kinetic assemblies occupy higher-energy local minima separated from the global minimum by activation energy barriers ( $E_a$ ).<sup>9–12</sup> These metastable states are inherently unstable and can transition toward the equilibrium state by overcoming the activation barrier, a process governed by the height of the

barrier itself.<sup>9–12</sup> If the barrier is sufficiently low, thermal energy at room temperature may be enough to drive the conversion spontaneously, classifying the assemblies as metastable.<sup>11</sup> However, when the barrier is too high, an external stimulus is required to induce transformation; otherwise, the system remains kinetically trapped for prolonged periods.<sup>9–12</sup>

The nature of this transformation provides key insights into the pathway complexity of the energy landscape. For instance, when a kinetic structure first dissociates into monomeric building blocks before forming the thermodynamic product, this indicates the presence of competitive pathways.<sup>8,9</sup> Conversely, a direct conversion into the equilibrium state—*via* reorganisation or structural rearrangement—suggests a single pathway. In either case, multiple intermediate kinetic species may exist, enabling the classification of assembly pathways as either serial or consecutive.<sup>8,9</sup>

Understanding and leveraging this complexity has opened new avenues for noncovalent synthesis.<sup>1,2,4–6,8</sup> For example, Stupp and co-workers demonstrated that the selective formation or avoidance of equilibrium and non-equilibrium structures could be controlled in peptide amphiphile systems *via* solvent processing.<sup>1,6</sup> In a notable study, they identified two

<sup>a</sup> Department of Chemistry, University of Warwick, Coventry CV4 7AL, UK.  
E-mail: s.perrier@warwick.ac.uk

<sup>b</sup> Warwick Medical School, University of Warwick, Coventry CV4 7AL, UK

<sup>c</sup> Faculty of Pharmacy and Pharmaceutical Sciences, Monash University, Parkville, VIC 3052, Australia



accessible energy landscapes depending on whether the system's ionic strength was above or below a critical threshold ( $I_c$ ).<sup>6</sup> Under thermodynamic control, high ionic strength ( $I > I_c$ ) favoured long  $\beta$ -sheet fibres, while low ionic strength ( $I < I_c$ ) produced short, randomly coiled fibres. Interestingly, by adjusting the solvent preparation conditions, they were able to alter the energy landscape to introduce kinetic traps, resulting in metastable short  $\beta$ -sheet fibres at high ionic strength and long  $\beta$ -sheet fibres at low ionic strength. These kinetic states, while non-equilibrium in nature, held functional significance: the long  $\beta$ -sheet fibres enhanced cell adhesion and survival, whereas the short fibres disrupted adhesion and induced cell death. Another example of pathway complexity in supramolecular systems was provided by Takeuchi and coworkers.<sup>2</sup> They showed that a kinetically formed product, accessed through a competitive pathway, could modulate the polydispersity of a thermodynamic product that grows *via* a cooperative mechanism.<sup>13,14</sup> Specifically, the kinetic species functioned as a reservoir of monomers, delaying spontaneous nucleation and elongation. Instead, growth proceeded in a living fashion upon addition of seeds, which incorporated monomers at their tips in a controlled manner. Moreover, the growth rate of the thermodynamic fibres was found to correlate linearly with the seed-to-monomer ratio, enabling precise regulation of fibre length.

In this study, we investigate the energy landscape governing the self-assembly of a polymer-conjugated  $\alpha$ -alt(D,L)-cyclic peptide system by monitoring time-resolved changes in the size distribution of the resulting supramolecular assemblies using asymmetric-flow field flow fractionation (AF<sub>4</sub>). Cyclic peptides with alternating D- and L-configurations and an even number of residues are well known to assemble into nanotubes *via* hydrogen-bond-driven  $\beta$ -sheet stacking.<sup>15–17</sup> Using the method of size distribution profiling, an approach which has been shown to distinguish between unassembled unimers and aggregated species to provide a clear view of assembly growth,<sup>18–20</sup> we showed that insights in the assembly mechanism of cyclic peptide nanotubes (CPNTs) can be obtained through combined analysis of molecular weight distributions and structural characterisation.<sup>21</sup> We also demonstrated the effects of conjugating amphiphilic diblock copolymers—introducing a hydrophobic segment adjacent to the peptide core—on assembly behaviour. The conjugates showed no detectable unimers after 24 hours of equilibration, as the hydrophobic domain shields peptide hydrogen bonds in aqueous media and prevent competitive H-bonds formation with water, thus strengthening the assembly.<sup>21,22</sup> Interestingly, at low hydrophobic content, two distinct nanotube populations were observed: single cyclic peptide polymeric nanotubes (SCPPNs), formed by individual peptide stacking, and multi-nanotube stacks (M-SCPPNs), resulting from terminal association of multiple SCPPNs.<sup>21,22</sup> The latter were proposed to arise from enhanced hydrogen bonding, possibly as a mechanism to reduce entropic penalties associated with solvent exposure.

Here, we expand on these findings by systematically mapping a theoretical energy landscape responsible for these assembly behaviours. Through time-resolved weight distribution analysis

obtained by AF<sub>4</sub>, we examine the formation sequence, inter-conversion dynamics, and relative abundance of these supramolecular species. Additionally, we demonstrate how alternative preparation protocols might introduce complexity into the assembly pathway, thereby addressing important gaps in our understanding of the underlying self-assembly mechanisms.

## 2. Results & discussion

### 2.1 Conjugate design

In our previous work, we systematically investigated a series of self-assembling cyclic peptides (CPs) conjugated with amphiphilic diblock copolymers to examine how varying the hydrophobic blocks surrounding the peptide influenced the stability of the resulting nanotubular structures.<sup>18</sup> The study revealed that the hydrophobicity introduced through molecular design played a critical role in modulating the balance between  $\beta$ -sheet hydrogen bonding among peptides and hydrophobic interactions. For clarity, we refer to the hydrophobic content of the polymers as low, medium, or high, relative to their hydrophilic character. As discussed in our previous work, at low hydrophobic content, self-assembly was primarily driven by hydrogen bonding, while the introduction of hydrophobic domains enhanced this association. However, once the hydrophobicity reached a medium level, the hydrophobic effect appeared to compete with hydrogen bonding, thereby disrupting or significantly hindering nanotube formation.<sup>18</sup> In the present study, we extend this investigation to explore the energy landscape of a model conjugate system whose self-assembly is known to be predominantly governed by  $\beta$ -sheet stacking.<sup>18</sup> This conjugate consists of an  $\alpha$ -alt(D,L)-cyclic peptide functionalised with two poly(butyl acrylate)-*block*-poly(dimethyl acrylamide) [p(BA)-*b*-p(DMA)] arms at a 10:90 mol% ratio. Details of the synthesis and characterisation of these compounds has been reported elsewhere.<sup>18,22</sup>

### 2.2 Experimental design

**2.2.1 Preparation protocols.** The currently established method for generating nanotube assemblies of amphiphilic CP-polymer conjugates in aqueous environments involves an initial dissolution step in a highly hydrogen bond (H-bond) competitive solvent, which serves to inhibit premature aggregation.<sup>23</sup> This step, ranging from a few minutes to several hours, is designed to ensure that the conjugates are fully molecularly dissolved and exist predominantly in their smallest, ideally unimeric, assembly state. Self-assembly is then triggered by the gradual addition of an aqueous solution. Since most of these H-bond-disrupting solvents are highly organic, only small quantities are used, or they are later removed, to ensure compatibility with potential biological applications.<sup>14,23–25</sup> The exclusive formation of nanotube structures *via* this approach has been previously confirmed for amphiphilic conjugates with low hydrophobic content.<sup>18,22</sup>

However, it has remained unclear whether this time-sensitive pre-dissolution step is essential for successful nanotube



formation. As demonstrated by other studies, the timing between the addition of solvents or additives can be a significant parameter that dictates the self-assembly outcome. Not only can this affect the activation or de-activation of non-covalent interactions, but it can also determine the conditions at which initial growth (nucleation) takes place and hence the rate of growth.<sup>11,25</sup>

One major concern with omitting the pre-dissolution step is the risk of premature intersubunit aggregation, a phenomenon reported in early studies on cyclic peptides.<sup>26,27</sup> This refers to an uncontrolled aggregation process that occurs before ordered self-assembly, typically driven by hydrophobic interactions where unimers spontaneously cluster into disordered aggregates to shield their hydrophobic blocks from water.<sup>18</sup> Given the slow kinetics of amphiphilic conjugate self-assembly, such premature aggregation could significantly affect the final assembly by reshaping the system's energy landscape.<sup>18,22</sup> Therefore, to investigate how preparation methods influence assembly pathways, we also tested a modified version of the standard protocol. In this adapted approach, the pre-dissolution step was omitted, and the two solvent phases were combined in rapid succession.

**2.2.2 Kinetic measurements.** The self-assembly energy landscape of the conjugate system under each preparation protocol was evaluated by tracking time-dependent changes in its structural distribution. This distribution was characterised by integrating prior structural knowledge with molecular weight measurements obtained using asymmetric-flow field-flow fractionation (AF<sub>4</sub>). The gentle, non-invasive separation afforded by AF<sub>4</sub> makes it particularly well-suited for analysing supramolecular assemblies. Moreover, by coupling AF<sub>4</sub> with multi-angle light scattering (MALS) and refractive index (RI) detectors, it is possible to determine the absolute molecular weight distribution and relative abundance of self-assembled structures.<sup>18,28–31</sup> Two sets of experiments were

carried out over different timescales to capture the temporal evolution of structural changes. In the first, sequential measurements were taken, with each run lasting 47 minutes, the full duration of the AF<sub>4</sub> separation protocol (refer to SI, Section B.4), to identify the minimum time required to detect notable changes. Based on the findings from this initial set, a second experiment was performed with extended intervals between measurements to further monitor the progression of structural transformations over time.

## 2.3 Energy landscapes

**2.3.1 Standard protocol.** To investigate the energy landscape following the standard preparation protocol, a 1 mg mL<sup>-1</sup> conjugate solution was prepared by pre-dissolving the conjugate for one hour in 5% dimethyl sulfoxide (DMSO), a hydrogen bond-disruptive solvent. Subsequently, 95% aqueous solvent was added to the unimer solution a few minutes prior to AF<sub>4</sub> analysis.

A dominant unimodal peak (population A) was consistently observed in the resulting fractograms for the length of the study (Fig. 2a and Fig. S1a, b). This peak corresponds to the formation of individual nanotubes, with  $N_{\text{agg}} \sim 23 \pm 6$ , as previously validated through polymer analogues, size estimations, and small-angle neutron scattering (SANS) analysis (Fig. S1e and Table 1).<sup>21</sup> Over time, a second population (B,  $N_{\text{agg}} \sim 52 \pm 6$ ) gradually emerged, with a third population (C,  $N_{\text{agg}} \sim 70 \pm 6$ ) appearing after around 12 hours (Fig. 2a). AF<sub>4</sub>-based molecular weight calculations showed that populations B and C correspond to approximately double and triple the size of population A, respectively, and are thus attributed to vertical stacking of individual nanotubes, which is consistent with previous findings.<sup>18,22</sup> From this point onward, individual nanotubes will be referred to as single cyclic peptide polymer nanotubes (SCPPNs), while vertically stacked assemblies will be termed multi-nanotube assemblies (M-SCPPNs).

**Table 1** Summary of the relative abundance (%); molecular weight limits and averages (UL, LL,  $M_w$ ,  $M_n$ ); and aggregation number ( $N_{\text{agg}}$ ) of each detected population following standard preparation

| Kinetic timepoint <sup>a</sup> | Peak           | Conc (mg mL <sup>-1</sup> ) | UL <sup>c</sup>     | LL <sup>c</sup>     | $M_w^c$             | $M_n^c$             | $N_{\text{agg}}^d$ |
|--------------------------------|----------------|-----------------------------|---------------------|---------------------|---------------------|---------------------|--------------------|
| 9 min                          | A              | 0.853                       | $3.611 \times 10^5$ | $1.885 \times 10^5$ | $2.658 \times 10^5$ | $2.470 \times 10^5$ | 16 ← 23 → 31       |
| 4 h                            | A              | 0.827                       | $3.823 \times 10^5$ | $2.216 \times 10^5$ | $2.947 \times 10^5$ | $2.789 \times 10^5$ | 19 ← 25 → 33       |
|                                | B <sup>b</sup> | —                           | —                   | —                   | —                   | —                   | —                  |
| 8 h                            | A              | 0.773                       | $3.316 \times 10^5$ | $1.857 \times 10^5$ | $2.545 \times 10^5$ | $2.387 \times 10^5$ | 16 ← 22 → 28       |
|                                | B              | 0.083                       | $6.875 \times 10^5$ | $5.161 \times 10^5$ | $6.094 \times 10^5$ | $5.127 \times 10^5$ | 44 ← 52 → 59       |
| 12 h                           | A              | 0.768                       | $3.437 \times 10^5$ | $1.990 \times 10^5$ | $2.589 \times 10^5$ | $2.452 \times 10^5$ | 17 ← 22 → 29       |
|                                | B              | 0.078                       | $6.259 \times 10^5$ | $4.914 \times 10^5$ | $5.605 \times 10^5$ | $5.541 \times 10^6$ | 42 ← 48 → 53       |
|                                | C              | 0.012                       | $8.786 \times 10^5$ | $7.236 \times 10^5$ | $8.166 \times 10^5$ | $8.105 \times 10^6$ | 62 ← 70 → 75       |
| 24 h                           | A              | 0.698                       | $2.589 \times 10^5$ | $1.585 \times 10^5$ | $2.065 \times 10^5$ | $1.963 \times 10^5$ | 14 ← 18 → 22       |
|                                | B              | 0.105                       | $5.007 \times 10^5$ | $3.703 \times 10^5$ | $4.321 \times 10^5$ | $4.261 \times 10^5$ | 32 ← 37 → 43       |
|                                | C              | 0.031                       | $8.911 \times 10^5$ | $7.038 \times 10^5$ | $7.731 \times 10^5$ | $7.322 \times 10^5$ | 60 ← 66 → 76       |
| 48 h                           | A              | 0.650                       | $2.809 \times 10^5$ | $1.659 \times 10^5$ | $2.183 \times 10^5$ | $2.081 \times 10^5$ | 14 ← 19 → 24       |
|                                | B              | 0.125                       | $5.144 \times 10^5$ | $3.921 \times 10^5$ | $4.362 \times 10^5$ | $4.309 \times 10^5$ | 33 ← 37 → 44       |
|                                | C              | 0.036                       | $8.703 \times 10^5$ | $6.759 \times 10^5$ | $7.517 \times 10^5$ | $6.838 \times 10^5$ | 58 ← 64 → 74       |

<sup>a</sup> Indicates the time elapsed between sample preparation and analysis. <sup>b</sup> Signal intensities were too low to perform calculations. <sup>c</sup> g mol<sup>-1</sup>;  $M_w$  &  $M_n$ : weight- and number-average molecular weights; UL and LL: upper and lower molecular weight limits used as a measure of dispersity. The limits denote where 75% of the peak distribution lies within  $\pm 2$  standard deviations ( $2\sigma$ ) away from the mean ( $M_w$ ), see SI, Section B.7.<sup>38</sup> <sup>d</sup> The  $N_{\text{agg}}$  range of the assemblies within the specified peak, calculated from the  $M_w$  (mean), UL (right,  $+2\sigma$ ) and LL (left,  $-2\sigma$ ); formula = ( $M_w$  value)  $\div$  theoretical  $M_w$  of conjugate unimer ( $1.173 \times 10^4$ ).



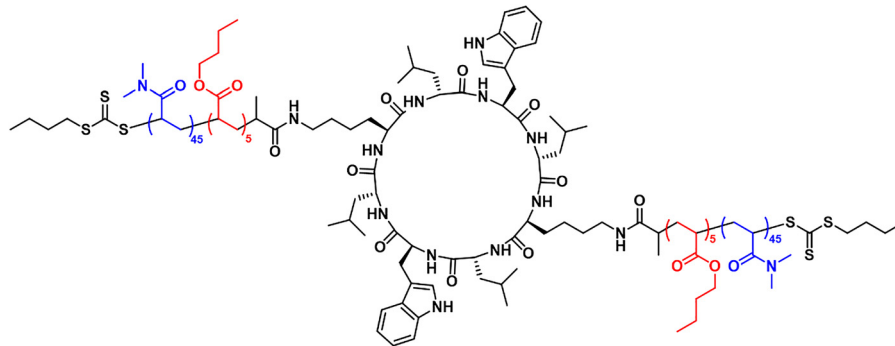


Fig. 1 Chemical structure of the investigated conjugate, CP-[p(BA)<sub>5</sub>-b-p(DMA)<sub>45</sub>]<sub>2</sub>. The conjugate consists of an  $\alpha$ -alt(D,L)-cyclic peptide with the following amino acid sequence: (D-Leu-L-Trp-D-Leu-L-Lys)<sub>2</sub> and poly(butyl acrylate, BA)-b-poly(dimethyl acrylamide, DMA) arms.

These results indicate that the transition from unimers to individual nanotubes occurs rapidly, beyond the temporal resolution of our experimental setup (on the order of minutes). This conclusion is supported by the absence of any detectable unimer population at the beginning of the measurement series, as well as the consistency in modality, dispersity, and average size across the early distributions of the single nanotube population (Fig. S1a, b and Table S1). Moreover, the self-assembly process appears to follow a sequential pathway through metastable intermediates, populations A and B, leading ultimately to the M-SCPPNs (Fig. 2b).<sup>9–12</sup> This is evidenced by the direct conversion of population A to B, followed by the progressive transformation of B to C over time.

The equilibrium structures are hypothesised to be the M-SCPPNs (population C), which, on average, comprise three stacked SCPPNs. This interpretation is based on the stability of these assemblies over extended periods with no further detectable reorganisation.<sup>9–12</sup> However, as the relaxation of kinetically trapped structures can span from minutes to several months,<sup>9</sup> a more nuanced view suggests that the true equilibrium state consists of M-SCPPNs with at least three stacked individual nanotubes. Crucially, the inferred shape of the energy landscape indicates a thermodynamic preference for assembling into longer nanotube stacks, driven by enhanced hydrogen bonding, and characteristic of a cooperative supramolecular system.

The slow accumulation of M-SCPPNs also provides insight into the presence of significant activation barriers to their formation (Table 1). These barriers likely arise from steric repulsion between the polymer shells of adjacent SCPPNs, which hinders stacking.<sup>7,32–34</sup> While direct quantification of these activation energies using Arrhenius analysis was not possible due to the absence of a temperature-controlled setup,<sup>35–37</sup> qualitative trends suggest that the activation barrier for the transition from A to B ( $E_{A1}$ ) is lower than that for B to C ( $E_{A2}$ ). This is inferred from the greater increase in population B relative to population C between 12 and 48 hours, despite concurrent transformation. Accordingly, the faster A  $\rightarrow$  B transition indicates a lower energy barrier, whereas the increasing steric hindrance with elongating structures likely results in higher activation barriers for further stacking steps.

These interpretations are consistent with prior observations: at 24 hours, single nanotubes dominated (78%), while populations B (17%) and C (5%) remained comparatively minor.<sup>18</sup>

**2.3.2 Comparison of assembling protocols.** In order to gain further insights on the assembling process, we investigated how altering the preparation protocol influences the self-assembly energy landscape. We compared our standard protocol with a method where the two solvents are added to the conjugates in rapid succession. Although the final solvent composition and the order of addition were consistent with the standard protocol, the resulting AF<sub>4</sub> fractograms displayed distinct differences (Fig. 3a). Notably, slight precipitation occurred upon the addition of the aqueous phase, and the first measurement revealed a broad, bimodal distribution. This structural profile suggests the coexistence of SCPPNs and disordered (D-) aggregates.

Population (1) (Fig. 3a) is attributed to SCPPNs, as indicated by the retention time of the refractive index (RI) signal, which aligns with the expected elution profile. This assignment is further supported by overlaying the 9-minute fractograms from both preparation protocols (Fig. S2a). In contrast, the presence of precipitation and the broad peak width (indicative of high polydispersity) point to the formation of disordered aggregates.<sup>18</sup> These D-aggregates are presumed to arise from hydrophobically driven, unregulated associations of amphiphilic unimers, characterised by inhomogeneous growth and substantial aggregation.<sup>18</sup> Additionally, the light scattering signal reveals a second population within the tail of the distribution, consistent with the presence of large, poorly soluble aggregates, as inferred from AF<sub>4</sub> elution principles and the noisy RI baseline.<sup>28–31</sup> These interpretations are corroborated by molecular weight analyses (Table 2), which confirm the expected size range for individual nanotubes at the peak and larger aggregates in the distribution tail.

We hypothesise that a portion of the conjugates sample was briefly solvated in pure DMSO, allowing those unimers to assemble into nanotubes *via* hydrogen bonding upon aqueous dilution. However, the remaining conjugates were exposed directly to the aqueous phase without prior molecular dissolution, causing hydrophobic interactions to dominate, and promoting uncontrolled aggregation.



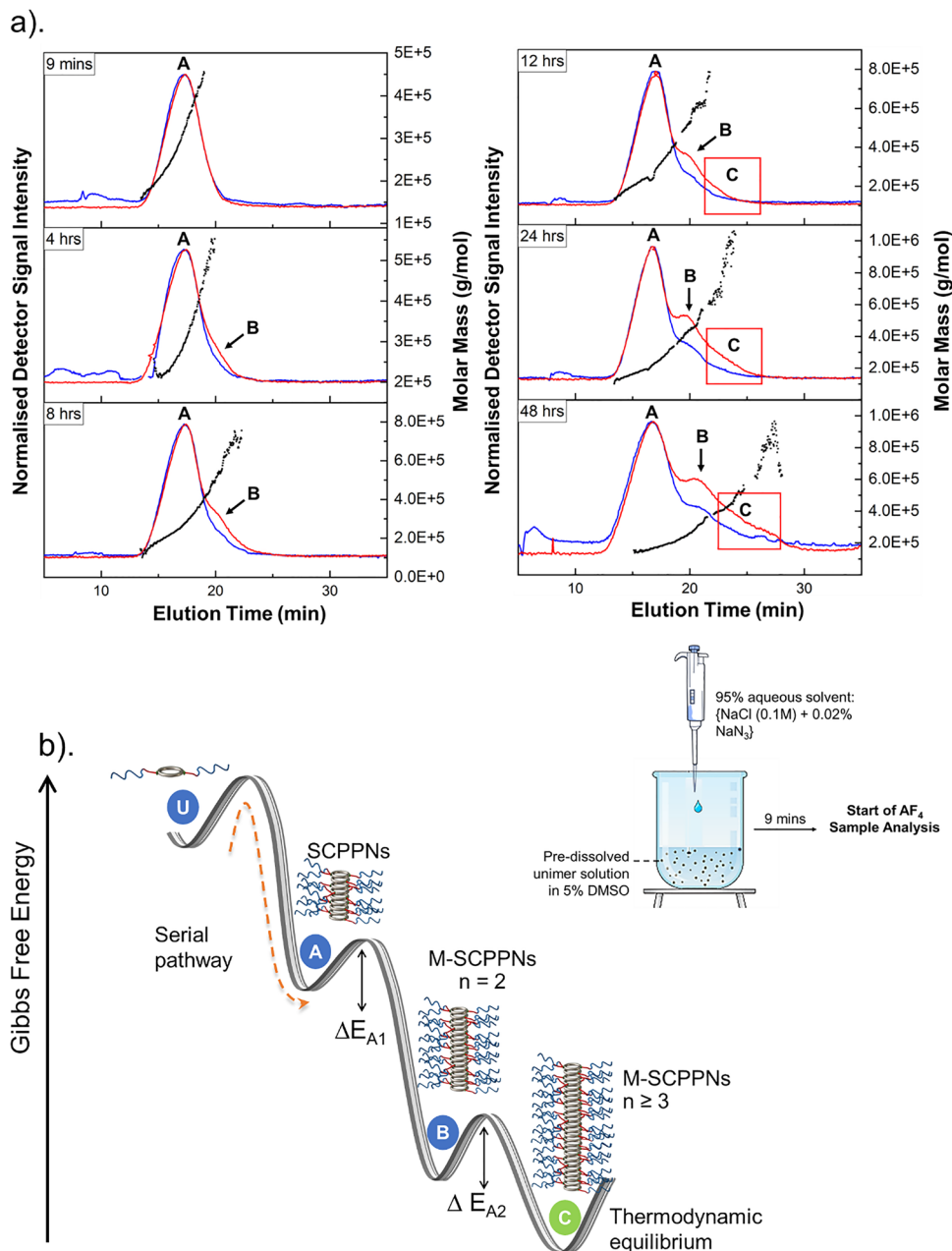


**Fig. 2** (a) Time-resolved AF<sub>4</sub>-MALS-RI fractograms of the amphiphilic conjugate (CP-[p(BA)<sub>5</sub>-b-p(DMA)<sub>45</sub>]<sub>2</sub>). The blue and red traces are the RI and MALS detector signals, respectively. The overlaid black traces (right y-axis) are the molecular weight values for each elution fraction, and the displayed time points indicate the time elapsed between sample preparation and analysis. (b) Schematic illustration of the theorised self-assembly energy landscape of the conjugate following standard preparation. The landscape is represented by a serial pathway with at least two metastable nanotube structures (A and B) and a thermodynamically favoured nanotube structure (C) with the highest  $N_{\text{agg}}$ . NB:  $n$  = average number of associating single nanotubes (SCPPNs) and  $E_{A1-2}$  are the activation barriers ascribed to stacking restrictions.

Remarkably, subsequent fractograms up to 48 hours showed a progressive increase in the concentration of SCPPNs, coinciding with a proportional decline in the D-aggregate population (Fig. 3a and Table 2). This shift led to a narrowing of the tailing distribution and the emergence of a unimodal, yet non-discrete, profile dominated by single nanotubes. Comparison of the dispersity values for the SCPPNs and tailing species at the final timepoint suggests that the remaining tailing population likely still consists of disordered aggregates rather than

multi-nanotube assemblies. This conclusion is based on a previously established trend showing that vertical stacking of SCPPNs leads to a decrease in dispersity – *i.e.*, M-SCPPNs exhibit lower dispersity than their single-nanotube counterparts.<sup>18</sup>

From these observations, several conclusions can be drawn. Most importantly, the disordered aggregates appear to be thermodynamically unstable and capable of dissociating into unimers, which can subsequently reassemble into SCPPNs. This is evidenced by the steady decline in D-aggregates and



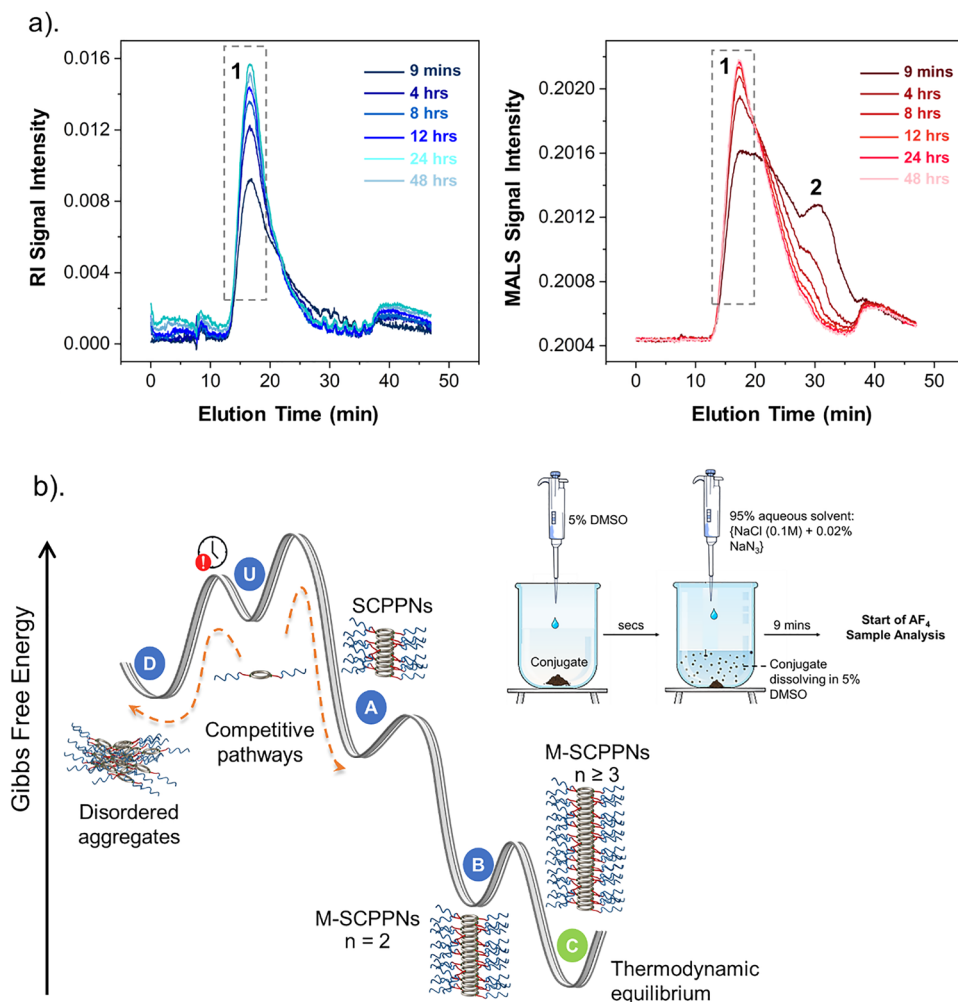


**Fig. 3** (a) Time-resolved AF<sub>4</sub>-MALS-RI fractograms of the amphiphilic conjugate (CP-[p(BA)<sub>5</sub>-b-p(DMA)<sub>45</sub>]<sub>2</sub>) following changes to the preparation protocol. The blue and red traces are the RI and MALS detector signals, respectively. (b) Schematic illustration of the proposed pathway complexity in the self-assembly energy landscape. Shortening the timing between solvent addition introduced a competitive, kinetically controlled pathway that results in the formation of metastable off-pathway intermediates (D-aggregates). These products act as a unimer trap which significantly retarded the formation of the thermodynamically favourable nanotube assemblies (M-SCPPNs). NB:  $n$  = average number of associating single nanotubes (SCPPNs).

the concurrent increase in single nanotubes. To test this inter-conversion hypothesis, a fresh conjugate solution was prepared *via* the standard protocol, and after SCPPN formation was confirmed, additional unimers were introduced. The resulting fractogram showed a proportional (2-fold) increase in the SCPPN population relative to the added unimers, thus validating the proposed mechanism (Fig. S2b and Table S2).

Taken together, these results suggest that the altered preparation method introduces a competing kinetic pathway in the self-assembly energy landscape (Fig. 3b).<sup>9–12</sup> This pathway, dominated by the formation of transient D-aggregates, is governed by hydrophobic interactions and likely represents an entropically favoured route. In contrast, the system ultimately favours formation of SCPPNs, indicating that their assembly follows a thermodynamically controlled process. Crucially, this preference implies that the conjugate's self-assembly in aqueous environments is not determined solely by solvent solvation effects, contrary to previous assumptions.<sup>18</sup>

Finally, the continuous disassembly of disordered aggregates throughout the experiment underscores the slow dynamics characteristic of this system – specifically, the slow rates of unimer dissociation and exchange.<sup>18,22</sup> This slow kinetic behaviour explains why correction toward the thermodynamic pathway occurs gradually and why the formation of multi-nanotube equilibrium structures remains significantly delayed within the timescale of measurement (*vide supra*).

**2.3.3 Insight gained on the self-assembly behaviour.** In this section, we revisit our prior understanding of the self-assembly behaviour of amphiphilic conjugates in light of the experimentally derived energy landscapes, which underscore the thermodynamic principles governing the assembly process. As previously proposed, the association behaviour of amphiphilic conjugates, and analogous systems, was interpreted as arising from different modes of solvent entropy compensation.<sup>18</sup> Here, for the first time, we interpret the evolution of the distinct nanostructures accessed through non-covalent interactions by



**Table 2** Summary of the relative abundance (%); molecular weight limits and averages (UL, LL,  $M_w$ ,  $M_n$ ); and aggregation number ( $N_{agg}$ ) of the populations detected the following preparation by the comparison protocol

| Kinetic timepoint <sup>a</sup> | Peak              | Conc (mg mL <sup>-1</sup> ) | UL <sup>c</sup>     | LL <sup>c</sup>     | $M_w^c$             | $M_n^c$             | $N_{agg}^d$    |
|--------------------------------|-------------------|-----------------------------|---------------------|---------------------|---------------------|---------------------|----------------|
| 9 min                          | 1                 | 0.247                       | $3.922 \times 10^5$ | $1.946 \times 10^5$ | $2.932 \times 10^5$ | $2.683 \times 10^5$ | 17 ← 25 → 33   |
|                                | Tail <sup>b</sup> | 0.293                       | $1.576 \times 10^6$ | $8.338 \times 10^5$ | $1.180 \times 10^6$ | $1.076 \times 10^6$ | 92 ← 101 → 134 |
| 4 h                            | 1                 | 0.354                       | $4.356 \times 10^5$ | $2.179 \times 10^5$ | $3.233 \times 10^5$ | $2.988 \times 10^5$ | 19 ← 28 → 37   |
|                                | Tail <sup>b</sup> | 0.268                       | $1.408 \times 10^6$ | $5.822 \times 10^5$ | $9.704 \times 10^5$ | $8.127 \times 10^5$ | 50 ← 83 → 120  |
| 8 h                            | 1                 | 0.381                       | $3.999 \times 10^5$ | $2.053 \times 10^5$ | $2.984 \times 10^5$ | $2.773 \times 10^5$ | 18 ← 25 → 34   |
|                                | Tail <sup>b</sup> | 0.244                       | $1.144 \times 10^6$ | $5.087 \times 10^5$ | $8.037 \times 10^5$ | $6.975 \times 10^5$ | 43 ← 69 → 98   |
| 12 h                           | 1                 | 0.406                       | $3.944 \times 10^5$ | $2.064 \times 10^5$ | $2.966 \times 10^5$ | $2.766 \times 10^5$ | 18 ← 25 → 34   |
|                                | Tail <sup>b</sup> | 0.223                       | $1.093 \times 10^6$ | $5.324 \times 10^5$ | $7.847 \times 10^5$ | $7.018 \times 10^5$ | 45 ← 67 → 93   |
| 24 h                           | 1                 | 0.426                       | $3.975 \times 10^5$ | $2.033 \times 10^5$ | $2.957 \times 10^5$ | $2.749 \times 10^5$ | 17 ← 25 → 34   |
|                                | Tail <sup>b</sup> | 0.213                       | $1.061 \times 10^6$ | $5.346 \times 10^5$ | $7.823 \times 10^5$ | $7.088 \times 10^5$ | 46 ← 67 → 90   |
| 48 h                           | 1                 | 0.435                       | $3.853 \times 10^5$ | $2.038 \times 10^5$ | $2.939 \times 10^5$ | $2.743 \times 10^5$ | 17 ← 25 → 33   |
|                                | Tail <sup>b</sup> | 0.205                       | $1.011 \times 10^6$ | $4.992 \times 10^5$ | $7.349 \times 10^5$ | $6.657 \times 10^5$ | 43 ← 63 → 86   |

<sup>a</sup> Indicates the time elapsed between sample preparation and analysis. <sup>b</sup> High molecular weight tail, including the population labelled 2. <sup>c</sup> g mol<sup>-1</sup>;  $M_w$  &  $M_n$ ; weight- and number-average molecular weights; UL and LL: upper and lower (respectively) molecular weight limits used as a measure of dispersity. The limits denote where 75% of the peak distribution lies within  $\pm 2$  standard deviations ( $2\sigma$ ) away from the mean ( $M_w$ ), see SI, Section B.7.<sup>38</sup> <sup>d</sup> The  $N_{agg}$  range of the assemblies within the specified peak, calculated from the  $M_w$  (mean), UL (right,  $+2\sigma$ ) and LL (left,  $-2\sigma$ ); formula = ( $M_w$  value)  $\div$  theoretical  $M_w$  of conjugate unimer ( $1.173 \times 10^4$ ).

framing the self-assembly process in terms of two fundamental requirements: (1) entropy compensation and (2) the attainment of thermodynamic equilibrium.<sup>9–12</sup>

To outline this hypothesis, we recall key thermodynamic principles:

(1) A negative Gibbs free energy change ( $\Delta G = \Delta H - T\Delta S$ ) is required to approach a system's minimum energy. Thus, under isothermal conditions, this necessitates a negative enthalpy change ( $\Delta H$ , e.g. bond formation) and a positive total entropy change ( $\Delta S_t = \Delta S_{system} + \Delta S_{solvent}$ );

(2) Changes in solvent entropy ( $\Delta S_{solvent}$ ) must be offset by opposing changes in system entropy ( $\Delta S_{system}$ ) such that  $\Delta S_{total}$  increases, in accordance with the second law of thermodynamics;

(3) The hydration of hydrophobic moieties imposes an entropic penalty on the solvent due to the ordering of water molecules. This penalty can be spontaneously compensated when these hydrophobic domains are sequestered ( $\Delta S_{system} \downarrow \ll \Delta S_{solvent} \uparrow = \Delta S_{total} \uparrow$ ).<sup>39–41</sup>

Based on these principles, we hypothesise that the initiation of self-assembly is driven by the need to offset the solvent entropy penalty, and that the nature of this initial regime significantly affects the system's progression toward a global energy minimum. Furthermore, as supported by the free energy landscapes, we propose that thermodynamic equilibrium is achieved through maximisation of hydrogen bonding among conjugates, which most effectively lowers  $\Delta G$ . This association is driven by the negative enthalpy of hydrogen bond formation and the positive entropy change by sequestering free hydrophobic unimers in solution.

We further postulate that solvent entropy loss can be compensated through two distinct mechanisms, the formation of disordered (D-) aggregates *via* the hydrophobic effect (a kinetically controlled pathway) or the formation of nanotube structures *via* hydrogen bonding (a thermodynamically controlled pathway).

In the latter case, hydrogen bonding does not directly satisfy the solvent's entropic requirement; rather, entropy compensation

is a consequence of the ordered H-bond-driven assembly. Importantly, we suggest that the primary role of the hydrophobic polymer region surrounding the peptide core (Fig. 1) is to shield the core from water molecules that would otherwise compete for hydrogen bonding. This shielding stabilises adjacent conjugate subunit interactions by enhancing and preserving hydrogen bonds.<sup>18,22,24,42,43</sup>

With respect to the pathway selected for entropy compensation, we propose that it is governed by the magnitude of the entropic penalty incurred when the conjugate is transferred into aqueous solution, *i.e.*, by the initial total entropy ( $S_{total, initial} = S_{system} + \Delta S_{solvent}$ ). This, in turn, depends on the solvent protocol and the overall hydrophobicity of the conjugate. Systems with low hydrophobic content and well-solubilised unimers have a smaller entropic cost than those with high hydrophobic content and no pre-dissolution. In the latter, both  $\Delta S_{solvent}$  and  $\Delta S_{system}$  are more negative.<sup>40</sup>

We therefore reason that higher entropic penalties favour the kinetic pathway, as D-aggregate formation involves lower activation barriers than the cooperative nucleation required for SCPPN formation, which is energetically less accessible.<sup>13,14,44–47</sup> Furthermore, the hydrophobic effect is a favourable compensatory mechanism, as it releases structured water without a significant loss in system entropy, *i.e.*  $\Delta S_{system}$  for disordered aggregation is less negative than that for highly ordered nanotube formation.

In conclusion, this study highlights the importance of system dynamics in achieving thermodynamic equilibrium in self-assembling conjugate systems. Our findings show that slow dynamics are favourable for hydrogen bonding and progression along the thermodynamic pathway, but unfavourable for switching from the kinetic to thermodynamic regime. Fundamentally, the molecular design of the conjugate governs its dynamics, influencing the dissociation and exchange rate of unimers in aqueous environments.<sup>18,22,24</sup> Specifically, a hydrophobic inner layer reduces unimer dissociation by shielding the hydrogen-bonding core from solvent disruption.<sup>18,22,24</sup> Similarly, trapping of unimers within D-aggregates is promoted



by high hydrophobicity, which favours unimer segregation over dissociation.

Thus, when low entropic cost is paired with high unimer exchange, the system favours nanotube formation and proceeds along the thermodynamic pathway. In contrast, when high entropic cost is coupled with restricted unimer mobility, the system becomes kinetically trapped in D-aggregates, hindering nanotube formation and delaying equilibrium. In both scenarios, increased hydrophobicity is expected to further suppress system dynamics, thereby amplifying these effects.

#### 2.4 Size dependency on concentration (dilution stability)

The earlier investigation into the interconversion behaviour of disordered (D-) aggregates suggested a potential relationship between the size of single nanotubes and the concentration of free unimers. Specifically, when additional unimers were introduced into a solution already containing SCPPNs, a slight

broadening of the nanotube distribution was observed, indicating minor elongation of some assemblies (Fig. S2b). However, subsequent size analysis revealed that this growth had minimal effect on the overall average size and dispersity of the nanotube population (Table S2). More notably, the principal consequence of increasing the unimer concentration was a proportional rise in the abundance of pre-existing nanotubes.

To examine the generality of these findings, two additional conjugate solutions were prepared at different concentrations (0.5 and 1 mg mL<sup>-1</sup>) using the standard protocol. The 0.5 mg mL<sup>-1</sup> solution was kinetically monitored to assess any changes in assembly dynamics, while the 1 mg mL<sup>-1</sup> solution was used to evaluate the structural stability of the nanotubes upon dilution. In the latter case, the solution was aged for 48 hours to allow for the formation of both SCPPNs and M-SCPPNs prior to a 2-fold dilution, after which the sample was re-analysed.

The kinetic AF<sub>4</sub> fractograms of the 0.5 mg mL<sup>-1</sup> solution revealed no significant differences in assembly behaviour compared to our previous results, with respect to both the rate of self-assembly and the types of structures formed (Fig. 4a). Similarly, the size and distribution characteristics of the assemblies remained consistent. For the diluted 1 mg mL<sup>-1</sup> sample, the results confirmed that the nanotube assemblies remained intact after dilution, with the only observable change being a reduction in measured concentration (Fig. 4b). This further supports the notion of slow system dynamics, underscoring one of the advantages of a thermodynamically governed assembly pathway.

Collectively, these results demonstrate that varying the unimer concentration within the limits set in this study, whether by mass or dilution, does not impact the size or structural integrity of the resulting nanotube assemblies, but only their detectable abundance. This confirms the structural robustness and dilution stability of these nanotubes, two essential characteristics for their potential application in biomedical contexts.<sup>16,48–51</sup>

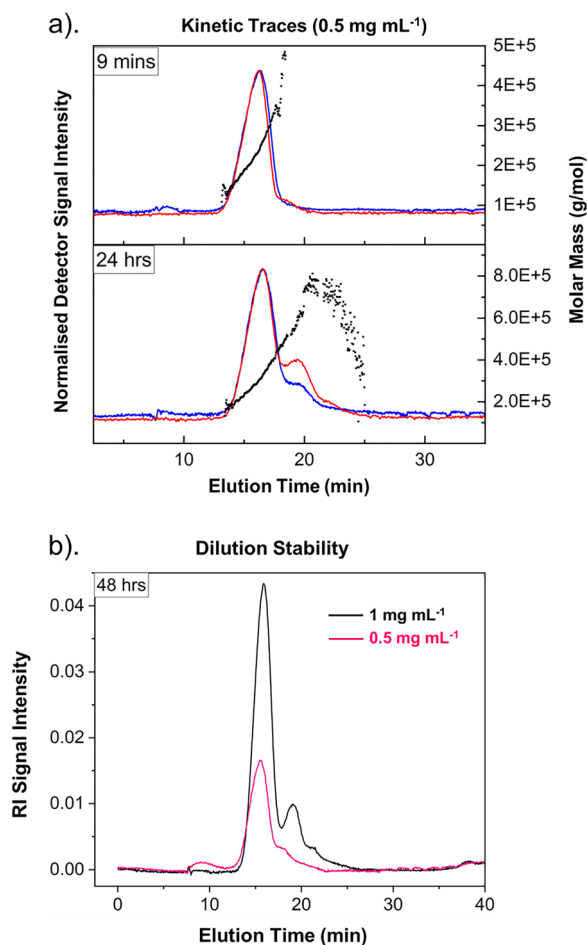


Fig. 4 (a) Time-resolved AF<sub>4</sub>-MALS-RI fractograms of the amphiphilic conjugate (CP-[p(BA)<sub>5</sub>-b-p(DMA)<sub>45</sub>]<sub>2</sub>) collected at a lower concentration (0.5 mg mL<sup>-1</sup>). The blue and red traces are the RI and MALS detector signals, respectively. The overlaid black traces (right y-axis) are the molecular weight values for each elution fraction and the displayed timepoints indicate the time elapsed between sample preparation and analysis. (b) Fractogram comparison of the structural distribution following a 2-fold dilution.

## Conclusion

This study has established the possible self-assembly energy landscape of a polymer-conjugated  $\alpha$ -alt(D,L)-cyclic peptide system and highlighted how both molecular design and preparation protocols influence the complexity and shape of this landscape. Our approach combined pre-existing structural insights with time-resolved molecular weight distribution measurements to monitor the formation and thermodynamic progression of the self-assembled structures.

In summary, our findings demonstrate that the global energy minimum is achieved through progressive hydrogen bonding between conjugate subunits, resulting in the formation of nanotubular assemblies. However, access to this thermodynamically favoured state is highly dependent on the dominant non-covalent interactions present at the onset of self-assembly. These initial interactions are governed by the need to compensate for solvent entropy loss incurred upon solvation of the conjugate's hydrophobic polymer segments. We propose that both the design of the conjugate and the solvent preparation protocol significantly influence the



magnitude of this entropy penalty, which in turn affects the balance between hydrogen bonding and the hydrophobic effect.

Specifically, when the entropic cost is low, the system is able to proceed along a thermodynamically controlled pathway driven by hydrogen bonding. Conversely, a higher entropic penalty favours a competing kinetic route governed by the hydrophobic effect, leading to the formation of metastable, disordered aggregates. Importantly, our results also show that the dynamic behaviour of the system, determined by the conjugate's molecular architecture, plays a critical role in reaching thermodynamic equilibrium. Slow dynamics are beneficial for stabilising hydrogen-bonded assemblies and guiding the system toward the equilibrium state. However, they simultaneously hinder the re-equilibration of off-pathway aggregates, thereby impeding the system's ability to transition from kinetic to thermodynamic regimes.

These slow dynamics also contribute to the exceptional morphological stability of the nanotube structures, making them particularly well-suited for biomedical applications where dilution stability and independence from concentration are desirable properties.<sup>16,48–51</sup>

This work establishes the first comprehensive thermodynamic framework for understanding the self-assembly of this class of cyclic peptide–polymer conjugates and demonstrates that AF<sub>4</sub> can be broadly adapted as a powerful analytical approach for other supramolecular systems, as diverse as  $\pi$ -stacking assemblies, peptide and protein nanofibers, block copolymer micelles and vesicles, hybrid organic–inorganic materials, and coordination-driven or hydrogen-bonded supramolecular polymers. As a next step, we aim to experimentally quantify key thermodynamic parameters ( $\Delta S$ ,  $\Delta H$ ,  $\Delta G$ , and  $E_A$ ) for each transition in the energy landscape. This will enable more precise control over the self-assembly process and further validate the theoretical concepts proposed in this study.

## Author contributions

M. K. conducted the AF<sub>4</sub> analyses and wrote the manuscript with the support of S. P. and J. Y. R. the conjugate design and synthesis protocol were developed by J. Y. R. synthesis and characterisation were performed by M. K. M. K. and S. P. performed data analysis and overall data interpretation.

## Conflicts of interest

The authors declare no competing interests.

## Data availability

The data supporting this article have been included as part of the supplementary information (SI). Supplementary information: The provided data includes additional characterisation data (AF<sub>4</sub> and SANS) and a description of the experimental protocols such as instrumental setup. See DOI: <https://doi.org/10.1039/d5ma00887e>.

## Acknowledgements

The authors would like to gratefully recognise the Molecular Analytical Science CDT (University of Warwick) and the Engineering and Physical Sciences Research Council for their financial support. We would also like to thank the following institutions for their kind equipment contributions: PostNova Analytics; the University of Warwick Research Technology Platform and the STFC ISIS Neutron and Muon Source Centre. Lastly, we thank Dr Stephen C. L. Hall (STFC ISIS) for the SANS structural characterisation data.

## References

- 1 P. A. Korevaar, C. J. Newcomb, E. W. Meijer and S. I. Stupp, Pathway Selection in Peptide Amphiphile Assembly, *J. Am. Chem. Soc.*, 2014, **136**(24), 8540–8543.
- 2 S. Ogi, K. Sugiyasu, S. Manna, S. Samitsu and M. Takeuchi, Living supramolecular polymerization realized through a biomimetic approach, *Nat. Chem.*, 2014, **6**(3), 188–195.
- 3 P. Khanra, A. K. Singh, L. Roy and A. Das, Pathway Complexity in Supramolecular Copolymerization and Blocky Star Copolymers by a Hetero-Seeding Effect, *J. Am. Chem. Soc.*, 2023, **145**(9), 5270–5284.
- 4 P. A. Korevaar, S. J. George, A. J. Markvoort, M. M. J. Smulders, P. A. J. Hilbers, A. P. H. J. Schenning, T. F. A. De Greef and E. W. Meijer, Pathway complexity in supramolecular polymerization, *Nature*, 2012, **481**(7382), 492–496.
- 5 P. A. Korevaar, T. F. A. de Greef and E. W. Meijer, Pathway Complexity in  $\pi$ -Conjugated Materials, *Chem. Mater.*, 2014, **26**(1), 576–586.
- 6 F. Tantakitti, J. Boekhoven, X. Wang, R. V. Kazantsev, T. Yu, J. Li, E. Zhuang, R. Zandi, J. H. Ortony, C. J. Newcomb, L. C. Palmer, G. S. Shekhawat, M. O. de la Cruz, G. C. Schatz and S. I. Stupp, Energy landscapes and functions of supramolecular systems, *Nat. Mater.*, 2016, **15**(4), 469–476.
- 7 P. Khanra, P. Rajdev and A. Das, Seed-Induced Living Two-Dimensional (2D) Supramolecular Polymerization in Water: Implications on Protein Adsorption and Enzyme Inhibition, *Angew. Chem., Int. Ed.*, 2024, **63**, e202400486.
- 8 P. K. Hashim, J. Bergueiro, E. W. Meijer and T. Aida, Supramolecular Polymerization: A Conceptual Expansion for Innovative Materials, *Prog. Polym. Sci.*, 2020, **105**, 101250.
- 9 J. Matern, Y. Dorca, L. Sánchez and G. Fernández, Revising Complex Supramolecular Polymerization under Kinetic and Thermodynamic Control, *Angew. Chem., Int. Ed.*, 2019, **58**(47), 16730–16740.
- 10 R. K. Grötsch and J. Boekhoven, Unique properties of supramolecular biomaterials through nonequilibrium self-assembly, in *Self-assembling Biomaterials*, ed. H. S. Azevedo and R. M. P. da Silva, Woodhead Publishing, 2018, pp. 235–250.
- 11 A. Sorrenti, J. Leira-Iglesias, A. J. Markvoort, T. F. A. de Greef and T. M. Hermans, Non-equilibrium supramolecular polymerization, *Chem. Soc. Rev.*, 2017, **46**(18), 5476–5490.



- 12 S. Dhiman and S. J. George, Temporally Controlled Supramolecular Polymerization, *Bull. Chem. Soc. Jpn.*, 2018, **91**(4), 687–699.
- 13 T. F. A. De Greef, M. M. J. Smulders, M. Wolffs, A. P. H. J. Schenning, R. P. Sijbesma and E. W. Meijer, Supramolecular Polymerization, *Chem. Rev.*, 2009, **109**(11), 5687–5754.
- 14 M. Hartlieb, E. D. H. Mansfield and S. Perrier, A guide to supramolecular polymerizations, *Polym. Chem.*, 2020, **11**(6), 1083–1110.
- 15 M. R. Ghadiri, J. R. Granja, R. A. Milligan, D. E. McRee and N. Khazanovich, Self-assembling organic nanotubes based on a cyclic peptide architecture, *Nature*, 1993, **366**(6453), 324–327.
- 16 J. Y. Rho and S. Perrier, 100th Anniversary of Macromolecular Science Viewpoint: User's Guide to Supramolecular Peptide–Polymer Conjugates, *ACS Macro Lett.*, 2021, **10**(2), 258–271.
- 17 Q. Song, Z. Cheng, M. Kariuki, S. C. L. Hall, S. K. Hill, J. Y. Rho and S. Perrier, Molecular Self-Assembly and Supramolecular Chemistry of Cyclic Peptides, *Chem. Rev.*, 2021, **121**(22), 13936–13995.
- 18 L. Yang, X. Tan, Z. Wang and X. Zhang, Supramolecular Polymers: Historical Development, Preparation, Characterization, and Functions, *Chem. Rev.*, 2015, **115**(15), 7196–7239.
- 19 Y. Liu, Z. Wang and X. Zhang, Characterization of supramolecular polymers, *Chem. Soc. Rev.*, 2012, **41**(18), 5922–5932.
- 20 M. M. Modena, B. Rühle, T. P. Burg and S. Wuttke, Nanoparticle Characterization: What to Measure?, *Adv. Mater.*, 2019, **31**(32), 1901556.
- 21 M. Kariuki, J. R. Rho, S. C. L. Hall and S. Perrier, Investigating the Impact of Hydrophobic Polymer Segments on the Self-Assembly Behavior of Supramolecular Cyclic Peptide Systems via Asymmetric-Flow Field Flow Fractionation, *Macromolecules*, 2023, **56**(17), 6618–6632.
- 22 J. Y. Rho, H. Cox, E. D. H. Mansfield, S. H. Ellacott, R. Peltier, J. C. Brendel, M. Hartlieb, T. A. Waigh and S. Perrier, Dual self-assembly of supramolecular peptide nanotubes to provide stabilisation in water, *Nat. Commun.*, 2019, **10**(1), 4708.
- 23 M. H. Abraham, P. L. Grellier, D. V. Prior, J. J. Morris and P. J. Taylor, Hydrogen bonding. Part 10. A scale of solute hydrogen-bond basicity using log K values for complexation in tetrachloromethane, *J. Chem. Soc., Perkin Trans. 2*, 1990, (4), 521–529.
- 24 J. Y. Rho, J. C. Brendel, L. R. MacFarlane, E. D. H. Mansfield, R. Peltier, S. Rogers, M. Hartlieb and S. Perrier, Probing the Dynamic Nature of Self-Assembling Cyclic Peptide–Polymer Nanotubes in Solution and in Mammalian Cells, *Adv. Funct. Mater.*, 2018, **28**(24), 1704569.
- 25 Y. Tidhar, H. Weissman, S. G. Wolf, A. Gulino and B. Rybtchinski, Pathway-Dependent Self-Assembly of Perylene Diimide/Peptide Conjugates in Aqueous Medium, *Chem. – Eur. J.*, 2011, **17**(22), 6068–6075.
- 26 L. Tomasic and G. P. Lorenzi, Some Cyclic Oligopeptide with S<sub>2n</sub> Symmetry, *Helv. Chim. Acta*, 1987, **70**(4), 1012–1016.
- 27 M. R. Ghadiri, J. R. Granja, R. A. Milligan, D. E. McRee and N. Khazanovich, Self-assembling organic nanotubes based on a cyclic peptide architecture, *Nature*, 1993, **366**, 324–327.
- 28 M. E. Schimpf, K. Caldwell and J. C. Giddings, *Field flow fractionation handbook*, Wiley-Interscience, New York, 2000.
- 29 G. Lespes, J. Gigault and S. Battu, Field Flow Fractionation, *Anal. Sep. Sci.*, 2015, **4**, 1143–1176.
- 30 S. Podzimek, *Light Scattering, Size Exclusion Chromatography and Asymmetric Flow Field Flow Fractionation: Powerful Tools for the Characterization of Polymers, Proteins and Nanoparticles*, John Wiley & Sons, New Jersey, 2011.
- 31 S. Podzimek, *Asymmetric Flow Field Flow Fractionation*, *Encyclopedia of Analytical Chemistry*, John Wiley & Sons, Ltd, 2012.
- 32 E. D. H. Mansfield, M. Hartlieb, S. Catrouillet, J. Y. Rho, S. C. Larnaudie, S. E. Rogers, J. Sanchis, J. C. Brendel and S. Perrier, Systematic study of the structural parameters affecting the self-assembly of cyclic peptide–poly(ethylene glycol) conjugates, *Soft Matter*, 2018, **14**(30), 6320–6326.
- 33 J. Couet, J. D. J. S. Samuel, A. Kopyshv, S. Santer and M. Biesalski, Peptide–Polymer Hybrid Nanotubes, *Angew. Chem., Int. Ed.*, 2005, **44**(21), 3297–3301.
- 34 J. Couet and M. Biesalski, Polymer-Wrapped Peptide Nanotubes: Peptide-Grafted Polymer Mass Impacts Length and Diameter, *Small*, 2008, **4**(7), 1008–1016.
- 35 N. J. Greenfield, Analysis of the kinetics of folding of proteins and peptides using circular dichroism, *Nat. Protoc.*, 2006, **1**(6), 2891–2899.
- 36 Z. A. Piskulich, O. O. Mesele and W. H. Thompson, Activation Energies and Beyond, *J. Phys. Chem. A*, 2019, **123**(33), 7185–7194.
- 37 S. Vyazovkin, Activation Energies and Temperature Dependencies of the Rates of Crystallization and Melting of Polymers, *Polym. Chem.*, 2020, **12**(5), 1070.
- 38 S. Harisson, The downside of dispersity: why the standard deviation is a better measure of dispersion in precision polymerization, *Polym. Chem.*, 2018, **9**(12), 1366–1370.
- 39 D. T. Haynie, *Biological Thermodynamics*, Cambridge University Press, Cambridge, 2nd edn, 2008.
- 40 M. Schauerl, M. Podewitz, B. J. Waldner and K. R. Liedl, Enthalpic and Entropic Contributions to Hydrophobicity, *J. Chem. Theory Comput.*, 2016, **12**(9), 4600–4610.
- 41 I. Rayment, Protein Structure, in *Encyclopedia of Physical Science and Technology*, ed. R. A. Meyers, Academic Press, New York, 3rd edn, 2003, pp. 191–218.
- 42 J. Cramer, X. Jiang, W. Schönemann, M. Silbermann, P. Zihlmann, S. Siegrist, B. Fiege, R. P. Jakob, S. Rabbani, T. Maier and B. Ernst, Enhancing the enthalpic contribution of hydrogen bonds by solvent shielding, *RSC Chem. Biol.*, 2020, **1**(4), 281–287.
- 43 J. Grdadolnik, F. Merzel and F. Avbelj, Origin of hydrophobicity and enhanced water hydrogen bond strength near purely hydrophobic solutes, *Proc. Natl. Acad. Sci. U. S. A.*, 2017, **114**(2), 322–327.
- 44 R. Chapman, M. L. Koh, G. G. Warr, K. A. Jolliffe and S. Perrier, Structure elucidation and control of cyclic



- peptide-derived nanotube assemblies in solution, *Chem. Sci.*, 2013, **4**(6), 2581–2589.
- 45 T. D. Clark, J. M. Buriak, K. Kobayashi, M. P. Isler, D. E. McRee and M. R. Ghadiri, Cylindrical  $\beta$ -Sheet Peptide Assemblies, *J. Am. Chem. Soc.*, 1998, **120**(35), 8949–8962.
- 46 K. Kobayashi, J. R. Granja and M. R. Ghadiri, Beta-Sheet Peptide Architecture: Measuring the Relative Stability of Parallel vs. Antiparallel Beta-Sheets, *Angew. Chem., Int. Ed. Engl.*, 1995, **34**(1), 95–97.
- 47 M. R. Ghadiri, K. Kobayashi, J. R. Granja, R. K. Chadha and D. E. McRee, The Structural and Thermodynamic Basis for the Formation of Self-Assembled Peptide Nanotubes, *Angew. Chem., Int. Ed. Engl.*, 1995, **34**(1), 93–95.
- 48 S. C. Larnaudie, J. Sanchis, T.-H. Nguyen, R. Peltier, S. Catrouillet, J. C. Brendel, C. J. H. Porter, K. A. Jolliffe and S. Perrier, Cyclic peptide-poly(HPMA) nanotubes as drug delivery vectors: In vitro assessment, pharmacokinetics and biodistribution, *Biomaterials*, 2018, **178**, 570–582.
- 49 V. Torchilin, Tumor delivery of macromolecular drugs based on the EPR effect, *Adv. Drug Delivery Rev.*, 2011, **63**(3), 131–135.
- 50 Z. Ahmad, A. Shah, M. Siddiq and H.-B. Kraatz, Polymeric micelles as drug delivery vehicles, *RSC Adv.*, 2014, **4**(33), 17028–17038.
- 51 S. C. Larnaudie, J. C. Brendel, I. Romero-Canelón, C. Sanchez-Cano, S. Catrouillet, J. Sanchis, J. P. C. Coverdale, J.-I. Song, A. Habtemariam, P. J. Sadler, K. A. Jolliffe and S. Perrier, Cyclic Peptide-Polymer Nanotubes as Efficient and Highly Potent Drug Delivery Systems for Organometallic Anticancer Complexes, *Biomacromolecules*, 2018, **19**(1), 239–247.

